Biointerface Research in Applied Chemistry
Open-Access Journal (ISSN: 2069-5837)

Article
Volume 13, Issue 5, 2023, 473
https://doi.org/10.33263/BRIAC135.473

Discovery of Natural Anti-Apoptotic Protein Inhibitor Using Molecular Docking and MM-GBSA Approach: An Anticancer Intervention

Sarbjit Dey [1], Atul Kumar Singh [1], Shashank Kumar [1,*]

[1] Molecular Signaling & Drug Discovery Laboratory, Department of Biochemistry, Central University of Punjab, Bathinda, Punjab, India; shashankbiochemau@gmail.com (S.K.);
* Correspondence: shashankbiochemau@gmail.com (S.K.);

Scopus Author ID 55749344800

Received: 11.07.2022; Accepted: 26.08.2022; Published: 27.12.2022

Abstract: Apoptosis is a programmed molecular phenomenon in normal cells, and "evading apoptosis" is a hallmark of cancer. Overexpression of anti-apoptotic BCL-2 promotes cancer cell survival, leading to tumor formation, its maintenance and progression, and further chemoresistance. Therefore, BCL-2 is considered an exciting drug target in clinical studies. The Cip/Kip family protein p21, which acts as an inhibitor of cyclin-CDK complexes, can also exert anti-apoptotic function and thus be involved in cancer initiation and progression. Preliminary research suggests that *Piper chaba* phytochemical(s) possess anticancer activity, but the underlying mechanism is yet to be established. For the first time, we explored *Piper chaba* phytochemicals for their anti-apoptotic protein (BCL-2 and p21) inhibition potential using molecular docking and MM-GBSA experiments. UC2288 and Venetoclax were known standards for BCL-2 and p21 proteins, respectively. We also explored the pharmacokinetics and drug-likeness properties of lead molecules using the SwissADME web tool. A total of 45 *P. chaba* phytochemicals were identified from published literature and docked at the drug-binding site of target proteins. Chabamide F, Piperchabaoside B, Piperundecalidiene, and Chabamide G showed ≥ binding affinity (-9.0 kcal/mole) than UC2288, while Brachystamide B showed lower binding affinity (-9.7 kcal/mole) than Venetoclax. MM-GBSA results revealed Chabamide F has a higher binding affinity for p21 than the standard compound. Therefore, *P. chaba* phytoconstituents qualify for further experiments on the drug discovery process to target anti-apoptosis proteins in cancer cells.

Keywords: apoptosis; anti-apoptotic inhibitors; cancer; *in silico*; phytochemical.

1. Introduction

Apoptosis is an essential type of cell suicide program in which a cell actively chooses a path toward death in response to particular stimuli [1-3]. In multicellular organisms, this critical event is carefully regulated to determine the fate of individual cells in a whole organism [4, 5]. Apoptosis can be induced in two ways. The extrinsic pathway is induced on the cell surface when a particular ligand binds to its death receptors, such as Fas (CD95), TRAIL receptors, DR3, DR6, and tumor necrosis factor receptor (TNFR) family proteins. This ligand-receptor interaction causes an intracellular change to promote the activation of adaptor proteins and the formation of death-inducing signaling complexes. As a result, initiator caspase-8 gets cleaved and activated, allowing downstream executioner caspases to orchestrate cell death [6, 7].

Furthermore, activated caspase 8 cleaves BH3-only protein BID to enhance the intrinsic pathway [8, 9]. The second pathway is the intrinsic or mitochondrial pathway which is triggered in response to various cytotoxic stresses such as DNA damage or uncontrolled cell proliferation [10]. BCL-2 family proteins control this pathway by regulating the outer mitochondrial membrane (OMM) permeability to permit the discharge of apoptogenic factor cytochrome c from the intermembrane space into the fluid matrix of cytoplasm. Next, cytochrome c attaches to APAF-1 in the presence of dATP and recruits an inactive procaspase 9 (initiator protein) to assemble the heptameric complex apoptosome. Activation of caspase 9 subsequently triggers effector caspases-3 and -7 to cleave hundreds of cellular proteins that ultimately lead to well-known morphological events of an apoptotic cell, including DNA fragmentation, nuclear fragmentation, and membrane blebbing [11, 12]. Several studies have been performed on the proteins BCL-2 and p21, which protect the cells from apoptosis. Several inhibitors developed against these proteins have shown toxicities and a lack of efficacies in experimental conditions. Therefore, it is essential to search for more effective and less toxic inhibitors of anti-apoptotic proteins.

The creeper plant *Piper chaba*, commonly known as Chui Jhal in India, belongs to the family 'Piperaceae'. Research findings showed that compounds isolated from this plant exhibit a wide range of biological actions, including anti-microbial, antitumor, antidiabetic, and immunomodulatory effects. [13]. The present study has been designed to identify the phytoconstituents in *Piper chaba* and screen those compounds against anti-apoptotic BCL-2 and p21 proteins for their inhibitory properties using *in silico* methods.

2. Materials and Methods

2.1. Software and servers.

The current study used various Bioinformatics tools such as MarvinSketch, Avogadro, Open Babel, Autodock Vina, Pymol, and Biovia Discovery studio visualizer. In addition, the data retrieval and its evaluation and analysis were done using internet servers/resources such as the Pubchem database of NCBI, Protein Data Bank, and SwissADME [14, 15].

2.2. Ligands identification, retrieval, and preparation.

The compounds in *Piper chaba* family were searched in the published literature [13]. The identified compounds' three-dimensional structures, standard anti-apoptotic inhibitors Venetoclax and UC2288, were obtained from the open chemistry database PubChem [16]. The compound piperundecalidiene (CAS Number: 88660-11-1) retrieved from the chemistry search engine (www.chemsrc.com) was drawn up using Marvin sketch software (www.chemaxon.com) and converted to a 3D structure using the Avogadro software.

The freely available software Open Babel version 3.1.1 was used to interconvert the downloaded structures from .sdf to .pdb format [17]. The PDB files were used as inputs in the Autodock tools 1.5.6. All active bonds were rendered non-rotatable after adding the Gasteiger-type polar hydrogen charges and merging the nonpolar hydrogens with the carbons. Next, the outputs were saved in pdbqt format for molecular docking.

2.3. Protein retrieval and preparation.

The three-dimensional crystallographic structures of BCL-2 (PDB-ID: 4MAN) with a resolution of 2.07Å and p21 (PDB-ID: 2X4Z) with a resolution of 2.10Å were downloaded from the RCSB protein data bank (www.rcsb.org) in PDB format. The structures were prepared using the Autodock version 1.5.2 tool by deleting existing ligands and H_2O molecules. Afterward, the protein structure was modified by assigning polar only hydrogen atoms and Kollman charges. This procedure was repeated for both proteins, which were then saved as .pdbqt files for molecular docking.

2.4. Molecular docking.

Docking experiments of the ligands to their protein targets were performed using the Autodock tool 1.5.2, which uses the Lamarckian genetic algorithm (LGA). The catalytic site of each protein was the input, which helped create a file with grid parameters using a grid box. A 3D grid was set to cover the entire internal groove of the protein receptor, allowing enough space for the ligands to move freely and get deposited. The grid spacing was set to 1 Å with the size set to 40×40×40 points on the X, Y, and Z axes. Grid centre was created using the following dimensions: X = -15.696, Y = 4.783, Z = 0.768 for BCL-2 and X = 14.037, Y = 30.01, Z = 54.451 for p21. The size of the grid points, however, varied depending on the size of the protein. For other docking parameters, default values of the software were used. The protein and ligand data and the grid box parameters in the configuration file were used for docking utilizing Autodock Vina, which employs the AMBER force field combined with an iterated local search global optimizer. The proteins remained rigid, while the ligands remained flexible throughout the docking experiments [18]. After calculating the binding affinities of the ligands for BCL-2 and p21, the compounds were ranked according to their affinity scores in kcal/mol. The pose with the highest negative value was selected to compare the in silico performance with standard inhibitors. The Biovia Discovery Studio Visualizer was used to identify interacting residues of the proteins with best-docked ligands for further analysis.

2.5. MM/GBSA energy calculation.

Following molecular docking, the Molecular Mechanics/Generalized Born Model and Solvent Accessibility (MM-GBSA) were performed to calculate the protein and protein-ligand binding energies (kcal/mol). Since the MM/GBSA binding energies are estimated as free energies, a more negative value indicates more significant binding [19, 20].

2.6. ADME study.

ADME toxicity prediction is important in drug discovery [21-23]. The compounds that showed a considerable binding affinity for BCL-2 and p21 were subjected to a web program known as SwissADME [24]. This freely available web tool was used to evaluate the physicochemical properties and ADME parameters, pharmacokinetics, and drug-likeness of the compounds under study.

3. Results and Discussion

3.1. The binding affinity of ligands with selected proteins.

Docking experiments revealed the ligands' binding affinities and inhibition constants with anti-apoptotic proteins. The results for both proteins were ranked according to the affinities (kcal/mol) for the phytochemicals and standard compounds in tables 4.2 and 4.3. A few of the ligands exhibited better binding potential than the standard compounds. From the results, Chabamide F, Piperchabaoside B, and Piperundecalidiene showed higher binding affinities (-9.8, -9.4, and -9.4 kcal/mol, respectively) for p21 compared to UC2288 (-9.0 kcal/mol) which is the standard inhibitor for this protein. For BCL-2, the compound Brachystamide B showed the highest affinity compared to the standard inhibitor Venetoclax (-9.4 kcal/mol). The affinity is based on the interactions between the anti-apoptotic proteins and ligands in addition to the binding energies of the complexes. The lowest binding energy or the one with the highest negative value indicates good affinity. The other parameter is the inhibition constant Ki (in µM), which tells about the potential of a compound to cause half-maximum inhibition. It is calculated using the formula: Ki = exp (affinity/RT), where exp stands for exponential, R indicates the universal gas constant (1.985×10^{-3} kcal/mol/K), and T indicates standard temperature (25°C or 298 K) (Ortiz et al., 2019).

Table 1. Docking scores of *Piper chaba* phytochemicals complexed with p21.

S. No.	Ligands	Affinity (kcal/mol)	Ki (µM)
1	Chabamide F	-9.8	0.064
2	Piperchabaoside B	-9.4	0.125
3	Piperundecalidiene	-9.4	0.125
4	Chabamide G	-9.0	0.247
5	UC2288	-9.0	0.247
6	β-sitosterol	-8.9	0.292
7	Sylvatine	-8.8	0.346
8	Piperchabamide C	-8.7	0.410
9	Brachystamide B	-8.6	0.485
10	Piperchabaoside A	-8.6	0.485
11	Piplartine dimer A	-8.6	0.485
12	N-isobutyl-(2E-4E-14Z)-eicosatrienamide	-8.5	0.575
13	Troglitazone	-8.5	0.575
14	Piperchabamide F	-8.4	0.680
15	Guineensine	-8.3	0.806
16	Piperchabamide D	-8.3	0.806
17	(2E-4E-14E)-N-Isobutylicosa-2-4-14-trienamide	-8.2	0.954
18	N-isobutyl-(2E-4E)-octadecadienamide	-8.2	0.954
19	Retrofractamide B	-8.2	0.954
20	(2E-4E)-N-(2-Methylpropyl)-octadeca-2-4-dienamide	-8.1	1.130
21	Piperanine	-8.0	1.338
22	Pipernonaline	-8.0	1.338
23	Sitosterol	-8.0	1.338
24	Chabamide K	-7.9	1.585
25	E-trans-piplartine	-7.9	1.585
26	Piperolein B	-7.9	1.585
27	E-cis-piplartine	-7.8	1.876
28	Pipercallosine	-7.7	2.222
29	Dehydropipernonaline	-7.6	2.631
30	Piperine	-7.6	2.631
31	Sesamin	-7.6	2.631
32	9-(3'-4'-methylenedioxyphenyl)-nona-2E-4E-8E-trienoic acid	-7.5	3.116
33	Retrofractamide A	-7.5	3.116
34	Retrofractamide C	-7.5	3.116
35	Piperchabamide E	-7.4	3.690
36	Trichostachine	-7.4	3.690

S. No.	Ligands	Affinity (kcal/mol)	Ki (µM)
37	Piperchabamide A	-7.1	6.127
38	Piperchabamide B	-7.1	6.127
39	Piperlonguminine	-7.1	6.127
40	Methyl piperate	-7.0	7.256
41	N-isobutyl-(2E-4E)-dodecadienamide	-7.0	7.256
42	Pellitorine	-6.7	12.049
43	N-isobutyl-(2E-4E)-decadienamide	-6.3	23.693
44	(E-E)-2-4-Decadienoic isobutylamide	-6.1	33.224
45	Pentylamine	-3.9	1369.825
46	Butylamine	-3.6	2274.687

Table 2. Docking scores of *Piper chaba* phytochemicals complexed with BCL-2.

S. No.	Ligands	Affinity (kcal/mol)	Ki (µM)
1	Brachystamide B	-9.7	0.076
2	Venetoclax	-9.4	0.125
3	Chabamide G	-9.2	0.176
4	Piperchabaoside B	-9.2	0.176
5	Troglitazone	-9.2	0.176
6	(2E-4E-14E)-N-Isobutylicosa-2-4-14-trienamide	-9.1	0.208
7	Chabamide F	-9.0	0.247
8	Sylvatine	-9.0	0.247
9	Piperchabamide C	-8.8	0.346
10	Piperundecalidiene	-8.8	0.346
11	Piperchabamide F	-8.6	0.485
12	Retrofractamide A	-8.6	0.485
13	Pipercallosine	-8.5	0.575
14	Piperolein B	-8.5	0.575
15	Sitosterol	-8.5	0.575
16	(2E-4E)-N-(2-Methylpropyl)-octadeca-2-4-dienamide	-8.4	0.680
17	N-isobutyl-(2E-4E-14Z)-eicosatrienamide	-8.4	0.680
18	β-sitosterol	-8.3	0.806
19	Piperchabamide B	-8.3	0.806
20	Piperchabaoside A	-8.3	0.806
21	Pipernonaline	-8.3	0.806
22	Retrofractamide B	-8.3	0.806
23	E-cis-piplartine	-8.0	1.338
24	Sesamin	-8.0	1.338
25	Guineensine	-7.9	1.585
26	N-isobutyl-(2E-4E)-octadecadienamide	-7.9	1.585
27	Piperchabamide E	-7.9	1.585
28	Retrofractamide C	-7.9	1.585
29	Piperine	-7.8	1.876
30	Dehydropipernonaline	-7.7	2.222
31	E-trans-piplartine	-7.7	2.222
32	Piperchabamide A	-7.7	2.222
33	Piplartine dimer A	-7.7	2.222
34	Trichostachine	-7.7	2.222
35	Piperanine	-7.6	2.631
36	Chabamide K	-7.5	3.116
37	Piperchabamide D	-7.5	3.116
38	Piperlonguminine	-7.5	3.116
39	9-(3’-4’-methylenedioxyphenyl)-nona-2E-4E-8E-trienoic acid	-7.4	3.690
40	Pellitorine	-7.4	3.690
41	Methyl piperate	-7.0	7.256
42	(E-E)-2-4-Decadienoic isobutylamide	-6.8	10.175
43	N-isobutyl-(2E-4E)-dodecadienamide	-6.6	14.268
44	N-isobutyl-(2E-4E)-decadienamide	-6.5	16.896
45	Pentylamine	-3.8	1622.124
46	Butylamine	-3.4	3189.770

3.2. Amino acid residues in protein-ligand interactions.

Table 4.4 depicts the amino acid residues of the proteins involved in hydrogen bonds and other hydrophobic interactions with the top four ligand molecules. The docking results revealed that Arg471 and Ala563 of protein p21 are involved in hydrogen bond interactions with lead molecule Chabamide F, while residues His432, Pro494, and Pro557 are engaged in other non-covalent interactions (Figure 4.2A and 4.2B). Arg534 and Asn517 are involved in hydrogen bond interaction with Piperchabaoside B and Chabamide G, respectively. There was no hydrogen bond found in the case of Piperundecalidiene. For the reference inhibitor UC2288, a hydrogen bond was observed with Ala402, while Glu396, Met395, Ala348, Val335, Leu447, Ala402, and Asp405 are involved in other non-covalent interactions (Figure 4.2C and 4.2D).

Similarly, the amino acid residues of BCL-2 involved in hydrogen bonds and other interactions with the standard inhibitor Venetoclax along with four ligand molecules were also shown in table 5**.** Arg143 of BCL-2 forms the hydrogen bond with the lead molecule Brachystamide B, while Ala97, Phe101, Tyr105, Tyr199, Asp137, and Glu133 were found in other interactions of the protein (Figure 4.3A and 4.3B). In the case of standard Venetoclax, Arg104 was involved in a hydrogen bond, while the residues Arg143, Arg104, Ala146, Ala97, and Tyr199 were engaged in other non-covalent interactions (Figure 4.3C and 4.3D).

Table 3. Amino acids and interactions involved in anti-apoptotic proteins and test compound binding.

Target	Ligand	H- bond Interaction	Other interactions
p21$^{Waf1/Cip1}$			
	Chabamide F	Arg471, Ala563	His432, Pro494, Pro557
	Piperchabaoside B	Arg534	Arg534, Leu535, Leu538, Leu553, Val554
	Piperundecalidiene		Phe461, Leu363, Lys350, Leu447, Ala348, Val335
	Chabamide G	Asn517	Tyr515, Pro514, Arg534
	UC2288	Ala402	Glu396, Met395, Ala348, Val335, Leu447, Ala402, Asp405
BCL-2			
	Brachystamide B	Arg143	Ala97, Phe101, Tyr105, Tyr199, Asp137, Glu133
	Chabamide G		Tyr105, Phe101, Met112, Phe109, Ala146, Leu134
	Piperchabaoside B	Gly142, Tyr199	Ala97, Tyr199, Gln96
	Troglitazone	Ala97	Tyr199, Val145, Ala97, Arg104, Tyr105, Phe101, Arg143
	Venetoclax	Arg104	Arg143, Arg104, Ala146, Ala97, Tyr199

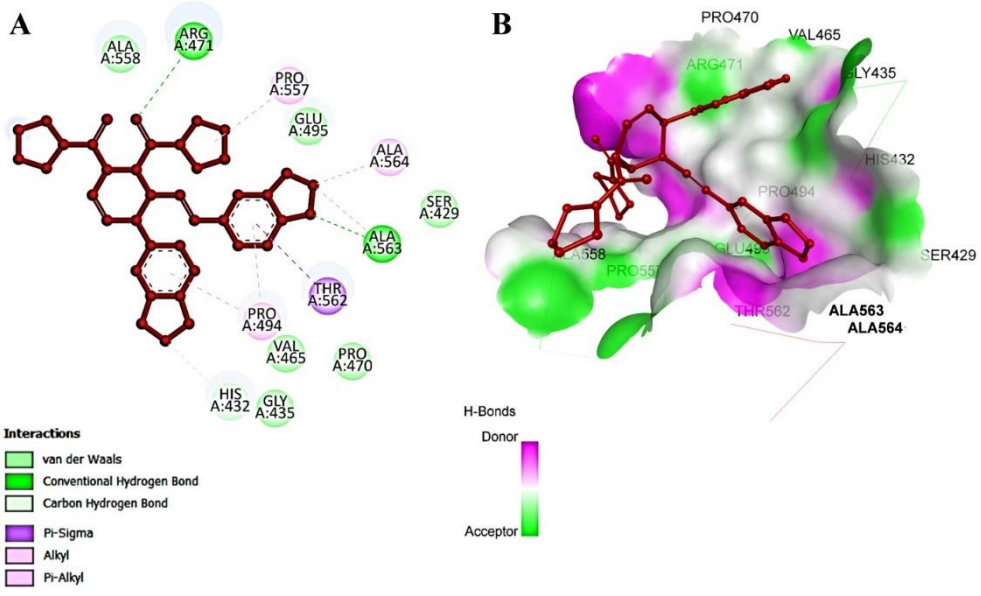

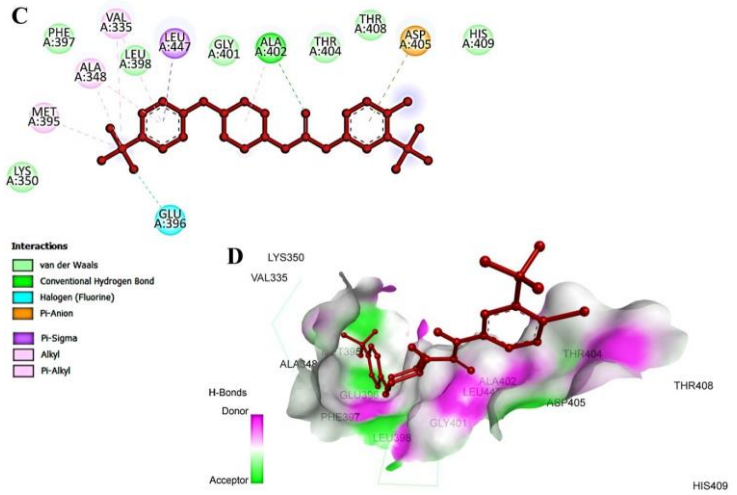

Figure 1. Ligand-protein interaction visualization**. (A)** Lead molecule (Chabamide F) - p21 interactions on a 2D diagram, and **(B)** receptor surfaces. **(C)** UC2288 - p21 interactions on a 2D diagram and **(D)** Receptor surfaces.

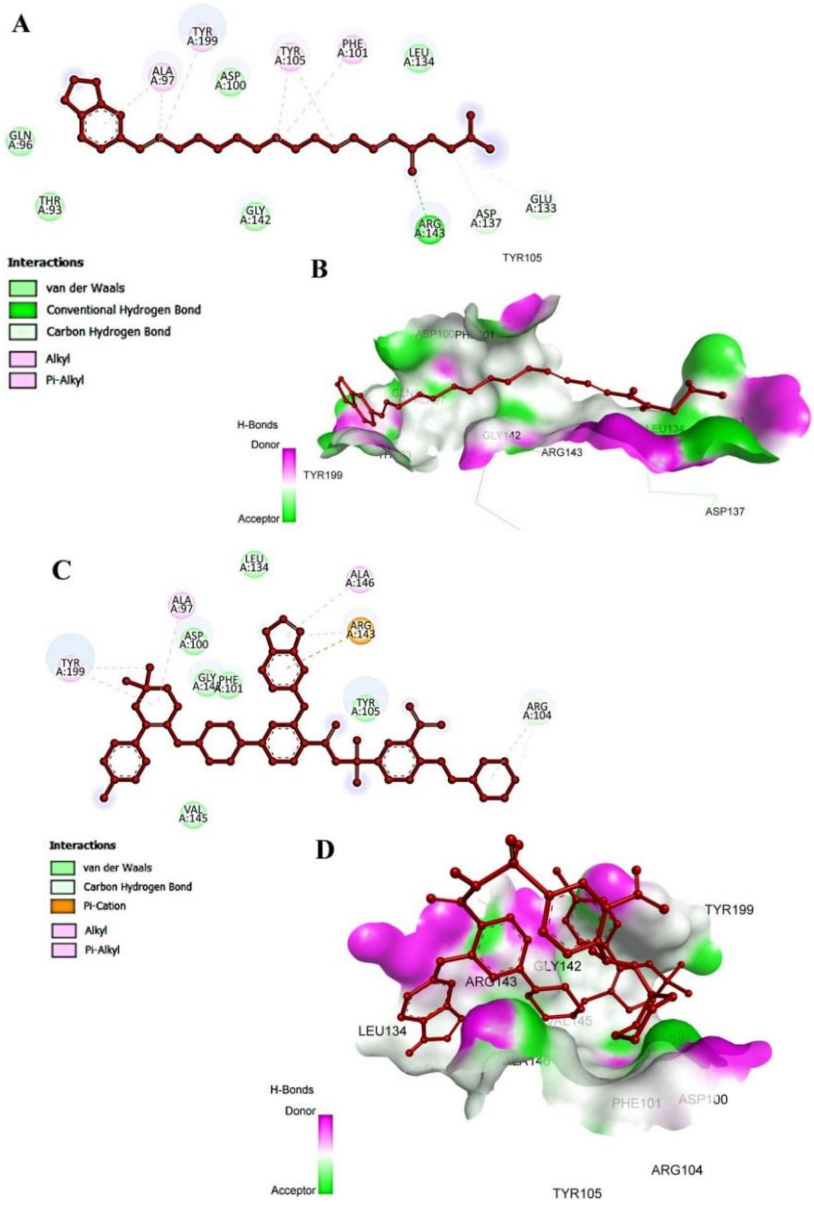

Figure 2. Ligand-protein interaction visualization. **(A)** Lead molecule (Brachystamide B and BCL-2 interactions on a 2D diagram, **(B)** receptor surfaces. **(C)** Venetoclax and BCL-2 interactions on a 2D diagram, **(D)** Receptor surfaces.

The following images were extracted using the Discovery studio visualizer. Figures 4.2A and 4.2C show the interactions of lead molecule Chabamide F and standard UC2288 with the p21 receptor on a 2D diagram. Amino acid residues involved in different interactions were shown in different colors. On the other side, figures 4.2B and 4.2D show the 3D receptor surfaces of p21 bound with Chabamide F and UC2288, respectively. Similarly, images were extracted for the protein BCL-2. Figures 4.3A and 4.3C show the interactions of lead molecule Brachystamide B and standard Venetoclax with the BCL-2 receptor on a 2D diagram. Amino acids involved in different types of interactions were shown in different colors. On the other side, figures 4.3B and 4.3D show the 3D receptor surfaces of BCL-2 bound with Brachystamide B and Venetoclax, respectively. The purple and green colors on the receptor surface indicate that the regions act as H-bond donors and acceptors.

3.3 Binding energy estimation of docked complexes

To get further insight into the comparative binding efficacy of Chabamide F and Brachystamide B to the catalytic domain of p21 and BCL-2, we estimated the binding energies of Chabamide F-p21 and Brachystamide B-BCL-2 complex by using the MM-GBSA approach. MM-GBSA approach is widely used to estimate the binding energies of protein-ligand complexes. MM-GBSA binding energy estimation also revealed the better binding efficiency of Chabamide F with p21 compared to UC2288 and Brachystamide B with BCL-2 compared to Venetoclax. Chabamide F exhibited binding energy of -51.27 Kcal/mole compared to UC2288, which showed binding energy of -36.90 kcal/mole (figures 4.4A and 4.4B). Brachystamide B had binding energy of -72.90 Kcal/mole compared to Venetoclax, which showed binding energy of -101.95 Kcal/mole (figures 4.5A and 4.5B).

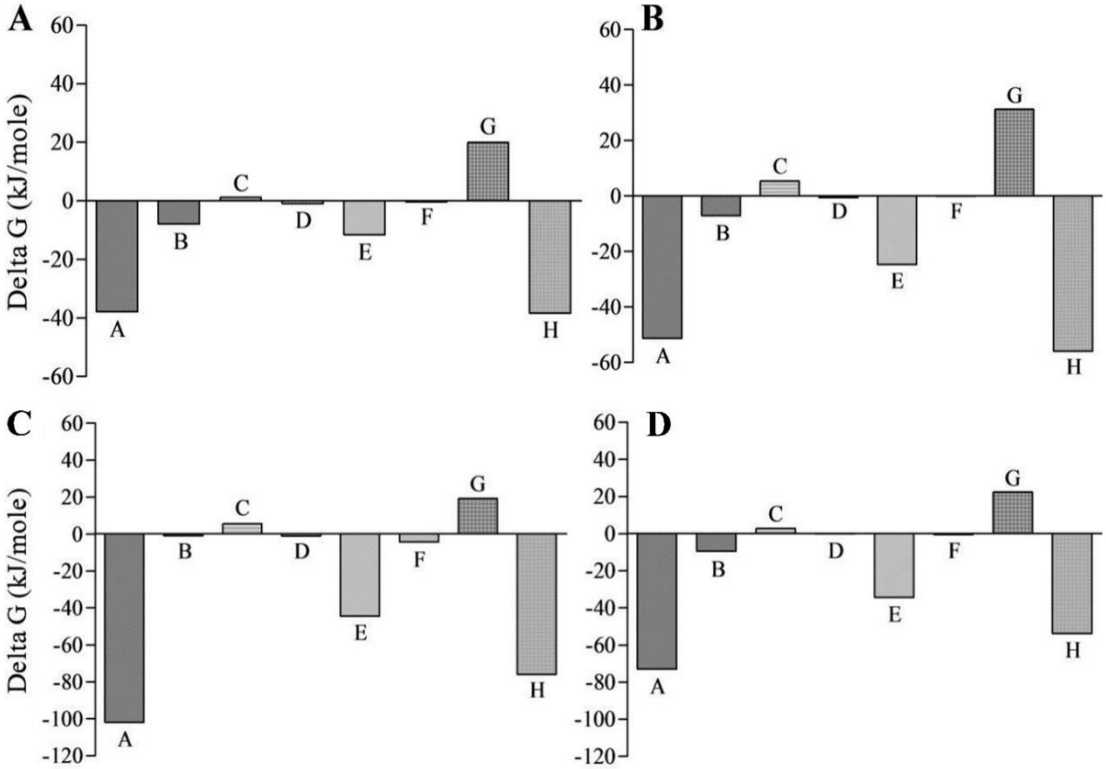

Figure 3. MM-GBSA calculations of **(A)** UC2288 and **(B)** Chabamide F in complex with protein p21. MM-GBSA calculations of **(C)** Venetoclax and **(D)** Brachystamide B in complex with BCL-2 protein. A. Total binding energy, B. Coulombic interaction energy, C. Covalent interaction energy, D. Hydrogen bond interaction energy, E. Lipophilic interaction energy, F. π-π packing interaction energy, G. Generalized Born electrostatic solvation energy, H. Van der Waals interaction energy.

Coulombic interaction energy, lipophilic interaction energy, and Van der Waals interaction energy were significant contributors to the total binding energy of both complexes. Both complexes showed similar contributions from the Van der Waals and lipophilic interaction energy. However, the significant difference in total binding energy comes from the Coulombic interaction energy, which was significantly higher for UC2288-p21 than the Chabamide F-p21. Based on dock score and MM-GBSA binding energy estimation, it can be stated that Chabamide F binds to the catalytic subunit of p21 more efficiently in comparison to the UC2288, and Brachystamide B binds less efficiently to BCL-2 in comparison to Venetoclax.

3.4. Pharmacokinetic and pharmacodynamics of lead molecules.

Different physicochemical properties such as formula, molecular weight, count of rotatable bonds, specific atom types, H-bond donors and acceptors, molar refractivity, and topological polar surface area (TPSA) of Chabamide F and Brachystamide B are provided in the table. To penetrate a cell, the TPSA value of a compound should be less than 90 $Å^2$. Pharmacokinetics represents the fate of a compound in a living system. GI stands for gastrointestinal absorption, and BBB indicates penetration of the blood-brain barrier (BBB). One of the crucial candidates of ABC-transporters is the P-GP or permeability glycoprotein, which evaluates the efflux of a molecule as a substrate or non-substrate of P-GP via the cell membrane. CYP represents cytochrome P450 that includes five isoforms – inhibition by certain compounds is a cause of drug-drug interactions. The log Kp parameter indicates the ability of a compound to penetrate the skin. The higher the negative value of log Kp, the lesser will be the penetration (Daina et al., 2017). Lastly, the drug-likeness includes the Lipinski parameter and bioavailability score. The Lipinski filter represents five sets of rules that state a compound shows insufficient absorption if there are: more than 10 H-bond acceptors (summation of Ns and Os), more than five H-bond donors (summation of OHs and NHS), the molecular weight is more significant than 500, and, logP is over 5 (or MLogP≥4.15) (Lipinski et al., 2001).

Table 4. Physiochemical, pharmacokinetics, and drug-likeness profile of the lead compounds.

	Chabamide F	**Brachystamide B**
Physicochemical properties		
Formula	$C_{32}H_{34}N_2O_6$	$C_{26}H_{37}NO_3$
Molecular weight	542.62 g/mol	411.58 g/mol
Num. heavy atoms	40	30
Num. arom. heavy atoms	12	6
Num. rotatable bonds	7	15
Num. H-bond acceptors	6	3
Num. H-bond donors	0	1
Molar refractivity	157.26	126.37
TPSA	77.54 $Å^2$	47.56 $Å^2$
Pharmacokinetics		
GI absorption	High	High
BBB permeant	Yes	No
P-gp substrate	Yes	Yes
CYP1A2 inhibitor	No	No
CYP2C19 inhibitor	Yes	No
CYP2C9 inhibitor	Yes	No
CYP2D6 inhibitor	No	No
CYP3A4 inhibitor	Yes	Yes
Log Kp (skin permeation)	-6.44 cm/s	-3.20 cm/s
Druglikeness		

	Chabamide F	Brachystamide B
Lipinski	Yes; 1 violation: MW>500	Yes; 1 violation: MLOGP>4.15
Bioavailability Score	0.55	0.55

Bioavailability radar plots of Chabamide F and Brachystamide B are shown in the figure. The pink on the radar diagram represents the area where a molecule must reside entirely to be considered a drug candidate. In other words, the pink area depicts the optimal range of each property. According to the diagram, the size of Chabamide F is quite large, whereas the flexibility, lipophilicity, and insolubility of Brachystamide B exceed the optimal range. Therefore, Chabamide F may be predicted as orally bioavailable but not Brachystamide B as it is too lipophilic, highly flexible, and nearly insoluble.

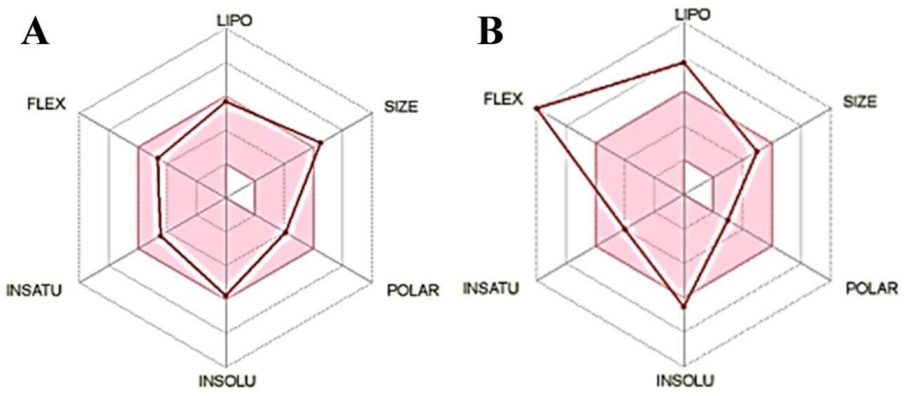

Figure 4. Bioavailability radar of lead molecules (**A**) Chabamide F; (**B**) Brachystamide B. Lipo - lipophilicity, Insole - Insolubility, Insitu - Instauration, Flex - rotatable bond flexibility.

4. Conclusions

In the present study, molecular docking experiments and MM-GBSA binding energy estimation were performed to identify novel natural inhibitors of targeted anti-apoptotic proteins BCL-2 and p21. Our study revealed that lead molecules, along with other phytoconstituents obtained from *Piper chaba*, have the potential to occupy the catalytic sites of BCL-2 and p21 proteins via hydrogen bonds and other non-covalent interactions. The MM-GBSA binding energy estimation showed the comparative binding energies of the lead molecules with the reference compounds against BCL-2 and p21 proteins. Docking studies highlighted that Chabamide F possesses remarkable inhibitory potential against p21, whereas Brachystamide B was identified as a lead molecule against BCL-2. The natural lead molecules identified in the current study should be tested *in vitro* and *in vivo* to understand their apoptosis-inducing potential.

Funding

This research received no external funding.

Acknowledgments

SK also acknowledges DST-India for providing a Departmental grant to the Department of Biochemistry, Central University of Punjab, Bathinda, India, in the form of a DST-FIST grant. AKS acknowledges CSIR, India, for providing a Senior Research Fellowship.

Conflicts of Interest

The authors declare no conflict of interest.

References

1. Tzifi, F.; Economopoulou, C.; Gourgiotis, D.; Ardavanis, A.; Papageorgiou, S.; & Scorilas, A. The role of BCL2 family of apoptosis regulator proteins in acute and chronic leukemias. *Adv Hematol.* **2012**, *2012*, 1-15, https://doi.org/10.1155/2012/524308.
2. Basu A. The interplay between apoptosis and cellular senescence: Bcl-2 family proteins as targets for cancer therapy. *Pharmacol Ther.* **2022**, *230*, 107943, https://doi.org/10.1016/j.pharmthera.2021.107943.
3. Koren, E.; Fuchs Y. Modes of Regulated Cell Death in Cancer. *Cancer Discov.* **2021**, *11*, 245-265, https://doi.org/10.1158/2159-8290.CD-20-0789.
4. Ros-Rocher, N.; Pérez-Posada, A.; Leger, M.M.; Ruiz-Trillo I. The origin of animals: an ancestral reconstruction of the unicellular-to-multicellular transition. *Open Biol.* **2021**, *11*, 200359, https://doi.org/10.1098/rsob.200359.
5. Mathavarajah, S.; VanIderstine, C.; Dellaire, G.; Huber R.J. Cancer and the breakdown of multicellularity: What Dictyostelium discoideum, a social amoeba, can teach us. *Bioessays.* **2021**, *43*, 2000156, https://doi.org/10.1002/bies.202000156.
6. Bertheloot, D.; Latz, E.; Franklin, B.S. Necroptosis, pyroptosis and apoptosis: an intricate game of cell death. *Cell Mol Immunol.* **2021**, *18*, 1106-1121, https://doi.org/10.1038/s41423-020-00630-3.
7. Bateman G, Hill B, Knight R, Boucher D. Great balls of fire: activation and signalling of inflammatory caspases. *Biochem Soc Trans*. **2021**, *49*, 1311-1324, https://doi.org/10.1042/BST20200986.
8. Loftus, L.V.; Amend, S.R.; Pienta, K.J. Interplay between Cell Death and Cell Proliferation Reveals New Strategies for Cancer Therapy. *Int J Mol Sci*. **2022**, *23*, 4723. https://doi.org/10.3390/ijms23094723.
9. Moujalled, D.; Strasser, A.; Liddell, J.R. Molecular mechanisms of cell death in neurological diseases. *Cell Death Differ*. **2021**, *28*, 2029-2044, https://doi.org/10.1038/s41418-021-00814-y.
10. Green, D. R. Cell death and the immune system: Getting to how and why. *Immunol Rev*. **2017**, *277*, 4–8, https://doi.org/10.1111/imr.12553.
11. Roberts, A.; Huang, D. Targeting BCL2 With BH3 Mimetics: Basic Science and Clinical Application of Venetoclax in Chronic Lymphocytic Leukemia and Related B Cell Malignancies: Basic science and clinical application of venetoclax. *Clin Pharm Therap*. **2017**, *101*, 89–98, https://doi.org/10.1002/cpt.553.
12. Zou, H.; Li, Y.; Liu, X.; Wang, X. An APAF-1.cytochrome c multimeric complex is a functional apoptosome that activates procaspase-9. *J Biol Chem*. **1999**, *274*, 11549–11556, https://doi.org/10.1074/jbc.274.17.11549.
13. Islam, M.T.; Hasan, J.; Snigdha, H.M.S..; Ali, E.S.; Sharifi-Rad, J.; Martorell, M.; Mubarak, M.S. Chemical profile, traditional uses, and biological activities of Piper chaba Hunter: A review. *J Ethnopharmacol.* **2020**, *257*, 112853, https://doi.org/10.1016/j.jep.2020.112853.
14. Prajapati, K.S.; Singh, A.K.; Kushwaha, P.P.; Shuaib, M.; Maurya, S.K.; Gupta, S.; Senapati, S.; Singh, S.P.; Waseem, M.; Kumar, S. Withaniasomnifera phytochemicals possess SARS-CoV-2 RdRp and human TMPRSS2 protein binding potential. *Vegetos.* **2022**, 1-20, https://doi.org/10.1007/s42535-022-00404-4.
15. Kushwaha, P.P.; Singh, A.K.; Bansal, T.; Yadav, A.; Prajapati, K.S.; Shuaib, M.; Kumar, S. Identification of Natural Inhibitors Against SARS-CoV-2 Drugable Targets Using Molecular Docking, Molecular Dynamics Simulation, and MM-PBSA Approach. *Front Cell Infect Microbiol.* **2021**, *11*, 730288, https://doi.org/10.3389/fcimb.2021.730288.
16. Kim, S.; Chen, J.; Cheng, T.; Gindulyte, A.; He, J.; He, S.; Li, Q.; Shoemaker, B.A.; Thiessen, P.A.; Yu, B.; Zaslavsky, L.; Zhang. J.; Bolton, E.E. PubChem in 2021: new data content and improved web interfaces. *Nucleic Acids Res*. **2021**, *49*, 388-395, https://doi.org/10.1093/nar/gkaa971.
17. O'Boyle, N. M.; Banck, M.; James, C. A.; Morley, C.; Vandermeersch, T.; Hutchison, G. R. Open Babel: An open chemical toolbox. *J Cheminform.* **2011**, *3*, 33, https://doi.org/10.1186/1758-2946-3-33.
18. Govindarasu, M.; Palani, M.; Vaiyapuri, M. (). In silico docking studies on kaempferitrin with diverse inflammatory and apoptotic proteins functional approach towards the colon cancer. *Int J Pharm Pharm Sci.* **2017**, *9*, 199, https://doi.org/10.22159/ijpps.2017v9i9.20500.
19. Gupta, S.; Singh, A.K.; Kushwaha, P.P.; Prajapati, K.S.; Shuaib, M.; Senapati, S.; Kumar, S. Identification of potential natural inhibitors of SARS-CoV2 main protease by molecular docking and simulation studies. *J Biomol Struct Dyn.* **2021**, *39*, 4334-4345, https://doi.org/10.1080/07391102.2020.1776157.

20. Shivakumar, D.; Williams, J.; Wu, Y.; Damm, W.; Shelley, J.; Sherman W. Prediction of Absolute Solvation Free Energies using Molecular Dynamics Free Energy Perturbation and the OPLS Force Field. *J Chem Theory Comput*. **2010**, *6*, 1509-1519. https://doi.org/10.1021/ct900587b.
21. Singh, A.K.; Kushwaha, P.P.; Prajapati, K.S.; Shuaib, M.; Gupta, S.; Kumar, S. Identification of FDA approved drugs and nucleoside analogues as potential SARS-CoV-2 A1pp domain inhibitor: An in silico study. *Comput Biol Med*. **2021**, *130*, 104185. https://doi.org/10.1016/j.compbiomed.2020.104185.
22. Rajkumar, M.; Maalmarugan, J.; Flora, G.; Surendarnath, S.; Christy, S.; Periyathambi, P.; Kumar, S,; Patel, R.P.; Lobo, F.D.; Singh, A.K.; Vimalan, M. Growth, characterizations, and the structural elucidation of diethyl-2-(3-oxoiso-1, 3-dihydrobenzofuran-1-ylidene) malonate crystalline specimen for dielectric and electronic filters, thermal, optical, mechanical, and biomedical applications using conventional experimental and theoretical practices. *J Mater Sci: Mater Electron*. **2021**, *32*, 22822-22839, https://doi.org/10.1007/s10854-021-06761-1.
23. Maalmarugan, J.; Divya, R.; Ganesan, H.; Patel, R.P.; Singh, A.K.; Kumar, S.; Vimalan, M.; SenthilKannan, K.; Dineshkumar, B. Synthesis, characterizations of D32DMBC-crystals for applications in biomedical, tribological, electronic filters and in device constructions by theory and practice. *J Nonlinear Opt Phys Mater*. **2022**, https://doi.org/10.1142/S0218863523500194.
24. Daina, A.; Michielin, O.; Zoete, V. SwissADME: a free web tool to evaluate pharmacokinetics, drug-likeness and medicinal chemistry friendliness of small molecules. *Sci Rep*. **2017**, *7*, 42717, https://doi.org/10.1038/srep42717.